Research Square

Preprints are preliminary reports that have not undergone peer review.
They should not be considered conclusive, used to inform clinical practice,
or referenced by the media as validated information.

H2-Ab1 deficiency in macrophages ameliorates spinal cord injury by regulating phagocytosis processing

Tianlun Zhao
Third Affiliated Hospital of Sun Yat-sen University
Yu Kang
Third Affiliated Hospital of Sun Yat-sen University
Haojie Zhang
Third Affiliated Hospital of Sun Yat-sen University
Senyu Yao
Third Affiliated Hospital of Sun Yat-sen University
Yang Yang
Third Affiliated Hospital of Sun Yat-sen University
Bin Liu
Third Affiliated Hospital of Sun Yat-sen University
Limin Rong
ronglm@mail.sysu.edu.cn
Third Affiliated Hospital of Sun Yat-sen University

Article

Keywords: Spinal cord injury, Macrophage, Phagocytosis, H2-Ab1, MHC Class II

Posted Date: October 30th, 2026

DOI: https://doi.org/10.21203/rs.3.rs-11316609/v1

License: This work is licensed under a Creative Commons Attribution 4.0 International License.
Read Full License

Additional Declarations: No competing interests reported.

Abstract

Recently, an increasing number of studies have highlighted the pivotal role of phagocytosis of macrophages/microglia following spinal cord injury, positioning it as a promising therapeutic target. The *H2-Ab1* gene encodes a part of the Major Histocompatibility Complex (MHC) Class II molecule, which is associated with cell activation and neuroinflammation. However, the specific functions and underlying mechanisms of *H2-Ab1* in spinal cord injury remain to be fully understood. Here, we utilized lineage tracing and found that the cellular localization of MHC Class II was predominantly expressed on infiltrating macrophages. Next, we employed macrophage/microglia conditional knockout mice to investigate the to investigate the role and potential mechanisms of MHC Class II in spinal cord injury. The results indicated that the deletion of *H2-Ab*1 in macrophages rather than microglia could improve the pathology following spinal cord injury. Furthermore, we demonstrated that *H2-Ab1* promotes the formation of foamy macrophages and drives their polarization toward the M1 phenotype. This process leads to increased secretion of inflammatory cytokines, which in turn induces the accumulation of reactive oxygen species (ROS) and enhanced neuronal apoptosis. More importantly, these findings may offer a promising clinical translation strategy based on the modulation of *H2-Ab1*.

Introduction

Spinal cord injury (SCI) is estimated to affect approximately 27 million people worldwide, making it a major cause of global disability [1]. About 90% of spinal cord injuries result from high-energy trauma, such as motor vehicle accidents, falls, and sports-related injuries [2]. Given the substantial physiological and economic burden associated with spinal cord injury (SCI) and the current lack of effective therapeutic strategies, there has been a growing focus among researchers on investigating the pathophysiology of SCI and exploring potential treatment approaches.

Traumatic spinal cord injury (SCI) can be divided into two stages: primary and secondary SCI [3]. Since primary SCI is difficult to reverse, most research has focused on the secondary stage of SCI [2, 4]. Secondary SCI is characterized by excessive phagocytosis, persistent inflammation, and extensive neuronal apoptosis. [5–7]. These pathological processes are closely interrelated [8–10]. Existing literature suggests that excessive phagocytosis of cellular debris and myelin fragments leads to the formation of foamy macrophages/microglia, which causes polarization imbalances, exacerbates inflammation, and ultimately results in widespread neuronal apoptosis [11–13]. Therefore, controlling excessive phagocytosis after SCI is crucial for effective treatment of spinal cord injury.

H2-Ab1 is a subunit of the major histocompatibility complex (MHC) Class II [14, 15] and is essential for the formation of the complex [16]. Studies have shown that MHC Class II molecules not only participate in antigen presentation but also play a role in regulating cell differentiation and activation [17, 18]. In the context of spinal cord injury, some researchers have proposed that it serves as a surface marker of pro-inflammatory M1 macrophages [19]. However, the role of H2-Ab1 and its potential mechanisms after spinal cord injury remain to be fully elucidated.

In this study, it was found that MHC Class II was associated with excessive phagocytosis, as shown by transcriptomics and immunoprecipitation-mass spectrometry (IP-MS). Since both resident macrophages (such as microglia) and peripheral macrophages (infiltrating macrophages) can express MHC Class II, to further investigate the localization of MHC Class II molecules after spinal cord injury, we bred $Cx3cr1^{CreER}$:R26-TdTomato mice (label microglia) and $Lyz2^{Cre}$:R26-TdTomato mice (label macrophage). We found that MHC Class II is primarily expressed in macrophages after spinal cord injury. Further, two types of conditional knockout mice ($Lyz2^{Cre}$:H2-$Ab1^{fl/fl}$ and $Cx3cr1^{CreER}$:H2-$Ab1^{fl/fl}$) were used to assess recovery from SCI and explore potential mechanisms. We found that knocking out *H2-Ab1* in macrophages, rather than in microglia, reduced the formation of foam macrophages and promoted the polarization of macrophages toward the M2 phenotype, thereby improving the inflammatory environment in the SCI region. This would lead to a reduction in ROS production in neurons, thereby decreasing neuronal apoptosis and ultimately improving recovery from spinal cord injury. In conclusion, we consider that the abnormal activation of *H2-Ab1* in macrophages after injury may be a potential target for clinical treatment of SCI.

Materials and method

Mice

Mice, including $Lyz2^{Cre+/-}$ (#004781), $Cx3cr1^{CreER+/-}$ (#021160), H2-$Ab1^{fl/fl}$ (#013181), and $Rosa26^{TdTomato+/+}$ (#007914) mice, all the C57BL/6 genetic background, were obtained from the Jackson Laboratory (Bar Harbor, ME, USA). $Lyz2^{Cre}$:R26-TdTomato mice were generated by crossing $Lyz2^{Cre+/-}$ with $Rosa26^{TdTomato+/+}$ mice, while $Cx3cr1^{CreER}$:R26-TdTomato mice from crossing $Cx3cr1^{CreER+/-}$ with $Rosa26^{TdTomato+/+}$ mice, $Lyz2^{Cre+/-}$:H2-$Ab1^{fl/fl}$ mice were generated by crossing $Lyz2^{Cre+/-}$ with H2-$Ab1^{fl/fl}$ mice. $Cx3cr1^{CreER}$:H2-$Ab1^{fl/fl}$ were generated by crossing $Cx3cr1^{CreER+/-}$ with H2-$Ab1^{fl/fl}$ mice. All transgenic mice mentioned have been genotyped. The $Cx3cr1^{CreER}$ mice were treated with intraperitoneal tamoxifen injections for five consecutive days (2.5 mg per mouse per day) when they were 4 weeks old [20]. All mice undergoing spinal cord injury were aged between 8 and 12 weeks. The primers used for identification are provided in **Supplementary Table 1**.

The animals were kept in the SPF (Specific Pathogen Free) Animal Core Facility of Sun Yat-sen University (#SYXK 2023 – 0112), with a 12 h cycle of light and darkness and unlimited access to water and food. Ethics application number: 2023003115.

Contusive spinal cord injury (SCI) surgery

Animals were anesthetized via intraperitoneal injections of sodium pentobarbital (30 mg/kg) followed by laminectomy at thoracic vertebra 9 (T9) and moderate (75-kdyn displacement) spinal cord compression with an Infinite Horizon Impactor (Precision Systems and Instrumentation, LLC, USA) using a tip with a diameter of 800 μm. The bladders were expressed once a day thereafter and the mice received

antibiotics and saline once daily for the first week [21]. The extent of injuries is controlled by Precision Systems and Instrumentation. All mice that survived the surgery and had contusions with recorded impact forces from 70 kD to 80 kD and displacements from 500 to 700 μm were included in the study. After surgery, mice received antibiotics and analgesics subcutaneously once daily for the first week.

Transcriptome sequencing and bioinformatics

Wild-type mice underwent contusive SCI surgery as described. After 3, 5, and 7 days, the spinal cords (5 mm segment containing injury epicenter, n = 3) were isolated for transcriptome sequencing. Intact spinal cords (5 mm segment with T9 as the center, n = 3) from mice treated only with laminectomy were used as controls. Library preparation and transcriptome sequencing were completed by Beijing Genomics institution (BGI). Gene set enrichment analysis (GSEA) was conducted on the transcriptomic data using an absolute value of the standardized enrichment score (NES) > 1 and adjusted p-value < 0.05 as criteria for significance. GeneMANIA (http://genemania.org/) was used to construct protein-protein interaction networks [22]. Accession to cite for these Sequence Read Archive data: PRJNA753793.

Protein extraction and Western blotting

Samples of spinal cord tissue (epicenter ± 0.5 cm) were lysed by ultrasonication in RIPA buffer with protease and phosphatase inhibitors (P1005, Beyotime, Shanghai, China). Protein concentrations were measured using a BCA kit (23225, Thermo Fisher, USA), and denatured samples in loading buffer were electrophoresed on 8–12% SDS-PAGE gels and electroblotted to PVDF membranes. Membranes were blocked in 5% BSA and treated with primary antibodies (4°C, overnight) before probing with secondary antibodies (1 h, room temperature (RT))[23]. Details of the antibodies are given in **Supplementary Table 2**. Signal intensities were detected with ECL and quantified by ImageJ software (v1.53a, NIH, USA).

RNA isolation and real-time quantitative PCR

Total RNA was extracted from spinal cord specimens with an E.Z.N.A. Total RNA Kit I (R6834-02 Omega, USA) and reverse-transcribed to cDNA with an Evo M-MLV kit (AG11705 Accurate Biology China) for qPCR. Amplification of 20 μl reaction volumes was performed using PowerUp TM SYBR TM Green Master Mix (A25742; Thermo Fisher) on a QuantS system (Applied Biosystems). Three independent runs with duplicates were used [24]. Gene expression was normalized to that of GAPDH using the $2^{-\triangle CT}$ method The qPCR primers are shown in **Supplementary Table 3**.

Immunofluorescence

The T9 spinal cord segments of anesthetized mice were completely removed after heart perfusion with saline and 4% paraformaldehyde (PFA). The spinal cord tissue was then embedded in OCT after 3 h of 4% PFA fixation and 2 days of gradient sucrose dehydration. The embedded tissue was cut into 20 μm

hick sections vertically or transversely with a microtome. The embedded tissue was cut into 20 μm thick sections either vertically or horizontally using a microtome. We collected tissue samples from an area 0.5 cm around the injury center and employed the microtome to make 20 μm serial sections. We collected tissue samples from 0.5 cm around the injury center and performed serial sectioning. In this experiment, all transverse and Coronal sections were identified by GFAP staining to determine the injury boundary, and confocal microscopy imaging was performed at the site of maximal injury. Images were acquired using LSM800 confocal microscope (Zeiss) or Dragonfly CR-DFLY-202 2540 (Leica). For tissue immunofluorescence staining, OCT on the tissue surface was rinsed off with PBS, sections were permeabilized in 0.4% Triton X 100 (solved in PBS buffer) for 2 h and blocked with 0.5% BSA (solved in PBS buffer) for 1 h, followed by treatment with primary antibodies overnight at 4°C. Next, secondary antibodies were incubated at RT for 2 h. Finally, sections were rinsed in water before mounting with ProLong Gold Antifade Reagent with DAPI (P36971, Thermo, USA) [25]. Details of the antibodies are given in **Supplementary Table 2**.

Cells were seeded onto coverslips and treated accordingly for each experiment. If necessary, fixation of cells occurred in 4% PFA for 15 mins. Subsequently, cells were incubated with fluorescent dyes according to manufacturer's instructions. The fluorescent dyes applied were listed in **Supplementary Table 2**. Images were taken using an inverted fluorescence microscope (Nikon, Japan).

scRNA-seq data sources and processing

Using the GEO database (https://www.ncbi.nlm.nih.gov/geo/) with the terms "spinal cord injury" and "single cell," we obtained dataset GSE162610 (uploaded by James S. Choi in 2020) [26]. This dataset comprises spinal cord tissue from mice collected at 4 time points, namely, uninjured and 1, 3 and 7 days post-injury, with sequencing on Illumina NextSeq 500 platform and annotation against Mus musculus.

Additionally, single-cell sequencing data were downloaded from https://doi.org/10.6084/m9.figshare.17702045.v2, including six time points after SCI, namely, 4 h, and 1, 3, 7, 14, and 38 days, as well as controls. The same sequencing platform was used [27].

Seurat v4.1.3 (https://satijalab.org/Seurat/) was used to analyze the sequencing data for data processing [28]. After quality control standardization and log transformation, genes showing significant variations were identified and used for principal component analysis (PCA). Both sets of sequencing data were integrated using Harmony. Clustering of the cells was performed using the first 30 principal components for t-distributed Stochastic Neighbor Embedding (tSNE) at 0.5 resolution. Unbiased cell type identification was conducted using SingleR, and cell types for each subgroup were identified in conjunction with the original annotations [29].

Basso Mouse Scale (BMS)

This scale was used for assessing mouse motor function following SCI. Mice were placed individually in an open area [30] and their movements over five mins were recorded by two independent blinded researchers on days 1, 3, 7, 14, 21, 28, and 35 post-SCI. Scoring ranged from 0, indicating no movement of the ankles, to 9, indicating full recovery, scored according to the movement of joints in the hindlimbs, position of the trunk, stability, paw placement, coordination of gait, toe clearance, and the position of the tail.

Motor evoked potential (MEP)

This was used to assess nervous system function in the hindlimbs on day 35 following SCI, using the BL-420A/F Data Acquisition Analysis System (TECHMAN SOFT). Electrodes were placed in the motor cortices and used to stimulate the brain, with the recording electrode positioned on the contralateral sciatic nerve. Motor neuron function was assessed by the amplitude of the first evoked peak.

Catwalk gait analysis

On day 35 following SCI, the mice were placed on a horizontal glass runway and their movements were recorded using a standard charge-coupled device (CCD) camera. Movements were analyzed using Catwalk software on a personal computer connected to the camera. Movements such as placement of paws, hindlimb support base, print and maximal areas, and swing speed were documented.

Immunoprecipitation-Mass Spectrometry (IP-MS)

Firstly, we performed spinal cord injury surgery on mice and collected samples seven days later. We extracted proteins from a 1 cm segment of spinal cord tissue at the injury site. After this processing, a co-immunoprecipitation (Co-IP) experiment targeting MHC Class II (14-5321-82, Invitrogen, USA) was conducted. The proteins obtained through immunoprecipitation were subsequently analyzed by mass spectrometry using a Q-Exactive HF-X mass spectrometer. During the experiment, a silica capillary C18 column (75 μm × 25 cm, Thermo, USA) was utilized for peptide separation. Mobile phase A consisted of a water solution containing 0.1% formic acid, while mobile phase B was composed of 80% acetonitrile with 0.1% formic acid. The flow rate was set at 300 nl/min. The obtained data were searched and compared against the UniProt database using MaxQuant software [31].

Oil Red O staining

Frozen Coronal spinal cord sections were immersed in 100% propylene glycol for 5 mins followed by staining with 0.5% Oil Red O (O0625, Sigma, USA) for 20 mins at 60°C. The sections were then treated with 85% propylene glycol (5 mins), washed (distilled water, three times).and examined and imaged under inverted microscopy (Nikon, Japan). The slice with the largest lesion area was selected for photography from the series of consecutive sections. ImageJ was used to quantification of stained areas.

BODIPY staining

To stain lipid droplets in spinal cord tissue, sections were washed with phosphate buffered saline and incubated with BODIPY 493/50 solution at RT for 15 mins. Nucleus was counterstained with 4’,6-diamidino-2-phenylindole (DAPI) for 5 mins at RT [32].

Flow cytometry

Initially, we harvested a 1-centimeter segment of spinal cord tissue from the injured region of an anesthetized mouse. Using a papain-based Neural Dissociation Kit (130-092-628, Miltenyi, Germany), the spinal cords were enzymatically dissociated to create single-cell suspensions. These cells were then resuspended in 200 µl of FACS buffer and blocked with FcR blocking reagent (Miltenyi, #130-092-575) prior to undergoing immunofluorescent staining for 20 mins at 4°C. Depending on the staining procedure, the cells were either fixed with 1% PFA for extracellular staining or permeabilized and fixed using the Foxp3/Transcription Factor Staining Buffer Set (eBioscience, #00-5523-00) before intracellular staining. The samples were analyzed using a Beckman flow cytometer, and the data were processed with FlowJo analysis software. A comprehensive list of flow cytometry antibodies is provided in **Supplementary Table 2.**

Transmission electron microscopy (TEM)

The mouse hearts were perfused with saline and 2.5% glutaraldehyde. Spinal cord tissues were harvested and placed in 2.5% glutaraldehyde overnight at 4°C. Following fixation, dehydration, and embedding, the tissues were cut into 70 nm sections and observed and imaged under TEM (HT7800/HT7700, Hitachi, Japan) [33].

Cell culture

Raw264.7 cells (Mouse macrophages) and Ht22 cells (mouse primary hippocampal neurons) were obtained from the American Type Culture Collection (ATCC; Rockville, MD, USA) and cultured in high-glucose Dulbecco's Modified Eagle Medium (DMEM; Invitrogen), supplemented with 10% fetal bovine serum (FBS; Invitrogen), 100 IU/mL penicillin (Invitrogen), and 100 µg/mL streptomycin (Invitrogen). All cells were maintained in a 37°C incubator with 5% CO_2 in a humidified atmosphere. For in vitro lipopolysaccharide (LPS) treatment, cells were exposed to 1 µg/mL LPS to simulate an inflammatory environment related to spinal cord injury. For the indirect co-culture experiment, we first treated RAW264.7 cells with 1 µg/mL LPS for 12 h, and then collected the cell supernatant. Based on the experimental groups, the supernatant was added to Ht22 cells in a 24-well plate, and after 24 h of incubation, the levels of reactive oxygen species (ROS) and apoptosis in Ht22 cells were assessed.

Phagocytosis assay

Carboxylate-modified fluorescent beads (FluoSpheres Carboxylate-Modified Microspheres (365/415; 505/515), ThermoFisher) were added (1.5 µl of a 1:10 dilution) and incubated for 2 h. Cells were then washed with ice-cold medium to arrest bead uptake, and immediately fixed with 4% PFA. After permeabilization with 0.4% Triton X-100 in PBS and blocking with 5% normal goat serum, cells were incubated with anti-Iba1 primary antibody, followed by anti-rabbit AlexaFluor 594 secondary antibody.

From each well, five 20x non-overlapping confocol images were taken from the top, middle, bottom, left and right areas. From each picture, the number of beads per cell was manually counted using Image J.

TUNEL assay

Frozen tissue sections and Ht22 cells were detected for apoptosis using the TUNEL Apoptosis Assay Kit (C1086-20T, Beyotime) according to the manufacturer's instructions. The nuclei were stained with DAPI, and images were acquired using an inverted fluorescence microscope (Nikon, Japan).

Dihydroethidium Staining

Frozen tissue sections and Ht22 cells were stained with DHE (470516A, Bestbio, China), following the manufacturer's guidelines. We stained the anterior horn of the transverse sections taken 2 mm rostral to the injury site and captured images using an inverted fluorescence microscope. The stained sections were evaluated quantitatively using ImageJ software to measure the integrated optical density of DHE.

Hematoxylin and eosin (H&E) staining

35 days after the surgery, the mice were deeply anesthetized and transcardially perfused, first with saline and then with 4% PFA. After embedding in OCT compound, the tissue was sectioned into 20 μm slices using a cryostat. The sections were stained with hematoxylin for 3–5 mins to stain the cell nuclei, followed by rinsing with tap water, and then stained with eosin for 1–2 mins to stain the cytoplasm. After staining, the sections were rinsed with water to remove excess dye, and then mounted using glycerol. Finally, the prepared slides were examined under a light microscope

Franz Nissl staining

OCT-embedded spinal tissues were cut longitudinally into 20 μm sections and stained with cresyl violet. The Nissl bodies in the sections were observed and imaged under microscopy (Nikon).

Statistical analysis

Data were analyzed using GraphPad Prism 9.0 (USA). Differences between two groups were assessed using a t-test, and those between multiple groups with two-way ANOVA. Data are shown as mean ± standard error of the mean (SEM). The level of significance defined as *P < 0.05, **P < 0.01, ***P < 0.001, ****P < 0.0001.

Result

The upregulation of MHC after spinal cord injury may be related to phagocytosis.

SCI can lead to a variety of pathophysiological processes and changes in gene expression [34]. Gene expression matrices at 3, 5, and 7 days after SCI were obtained *via* RNA sequencing. The top 10 pathways (ranked by adjusted p-value) are provided in Figure S1A-C. Phagosome pathways were enriched at all time points (D3: NES = 1.86; D5: NES = 1.89; D7: NES = 1.86, NES: Normalized Enrichment Score) and 70 genes were identified that were common to these three time points (Fig. 1A). A Protein-

Protein Interaction (PPI) network was constructed utilizing these 70 genes, and we found that the H2 family occupies a central position within this network. We identified that the top three functions enriched in the H2 family genes within this network are antigen processing and presentation, processing and presentation of peptide antigen, and MHC protein complex, all of which are associated with phagosome pathways (Fig. 1B). The distribution of H2 family genes in phagosome pathways and their expression at the three time points were then investigated (Fig. 1C-F), showing that the top three genes (ranked by Log2FC) were *H2-Ab1*, *H2-Aa*, and *H2-Eb1*. *H2-Ab1*, *H2-Aa*, and *H2-Eb1* are all subunit genes of MHC Class II and are related to the functions of MHC Class II. Among the MHC Class II subunit genes, *H2-Ab1* has been the most extensively studied and is considered as one of the essential genes for the assembly of MHC Class II.

MHC Class II is primarily expressed by macrophages on 7 days after SCI

To further investigate the cellular localization of H2-Ab1 after SCI, two single-cell RNA sequencing datasets were downloaded and analyzed [26, 27]. The results indicated that *H2-Ab1* was expressed in macrophages and microglia following SCI (Figs. 2A, B). It was also found that *H2-Ab1* expression was highest in subacute phase after SCI (Figs. 2C). The predominant cell types in and around the injured area after spinal cord injury are macrophages/microglia, astrocytes, oligodendrocytes, and neurons. Macrophages/microglia are indicated by the marker Iba1, astrocytes by GFAP, oligodendrocytes by myelin basic protein (MBP), and neurons by NeuN. Spinal cord sections taken 7 days after spinal cord injury were used for immunofluorescence analysis (Figs. 2D). We conducted a colocalization analysis between MHC Class II molecules and Iba1, GFAP, MBP, and NeuN (in the white boxed areas) (Figs. 2E-H). We found that the colocalization of MHC Class II with Iba1 was the most prominent. This indicates that MHC Class II is localized in macrophages and microglia.

MHC Class II levels following SCI were further analyzed by qPCR and western blotting of tissue at the lesion site on days 3, 7, 14, and 35 post-SCI. Relative to the sham group, *H2-Ab1* mRNA and protein levels were markedly upregulated in the SCI mice, reaching a maximum on 7 days after SCI (Fig. 2A-C). Next, immunofluorescence at the spinal cord cross-section was performed after spinal cord injury (Fig. 2D). Immunofluorescence analysis of cross-sections confirmed these findings (Fig. 2E). Interestingly, MHC Class II was in the center and around the damaged area. It is well-known that distinguishing between resident microglia and infiltrating macrophages is often difficult in terms of morphology and surface markers [35]. To investigate which cell type expresses the highest level of MHC Class II, we performed MHC Class II immunostaining on spinal cord sections from Cx3cr1^{CreER}:R26-TdTomato mice (mainly labeling microglia) and Lyz2^{Cre}:R26-TdTomato mice (mainly labeling macrophages) mice (Fig. 2F, G). Among the MHC Class II^{+} cells in Lyz2^{Cre}:R26-TdTomato mice, 68.4% are MHCII^{+} TdTomato^{+} cells (Fig. 2H). However, Among the MHC Class II^{+} cells in Cx3cr1^{CreER}:R26-TdTomato mice, 21.5% are MHCII^{+} TdTomato^{+} cells (Fig. 2I). Additionally, we found a significant difference in the area of co-staining

between the two fluorescent reporter mouse models. (Fig. 2J). Although the Cx3cr1^{CreER}:R26-TdTomato mice (designed to primarily label microglia) exhibit limited macrophage labeling and the Lyz2^{Cre}:R26-TdTomato mice (designed to primarily label macrophage) show minor microglial labeling, our experimental evidence indicates that MHC Class II molecules are preferentially highly expressed in macrophages.

Knockout of H2-Ab1 in macrophages promotes neural recovery following SCI

To investigate the effect of *H2-Ab1* on spinal cord injury, we generated two conditional knockout mouse models (Lyz2^{Cre}:H2-Ab1$^{fl/fl}$ and Cx3cr1^{CreER}:H2-Ab1$^{fl/fl}$) [36]. Knockout of *H2-Ab1* in macrophages (Lyz2^{Cre}) and microglia (Cx3cr1^{CreER}) was confirmed at both the DNA and protein levels (Figs. 3B, E). The experimental protocols are provided in the Supplementary Information (Figs. 3A, C), and the knockout did not affect the development of the mice (Figs. 3D). SCI was performed using the Infinite Horizon Impactor with an 800 μm tip. To assess the effects of *H2-Ab1* knockout on recovery of motor function, BMS scores, Catwalk gait analyses, and MEPs were measured. Lyz2^{Cre}:H2-Ab1$^{fl/fl}$ mice showed better recovery in the BMS score relative to the controls (Fig. 3A). We found that this better recovery began 7 days after spinal cord injury. It is suggested that this could be associated with the first peak of macrophage infiltration at day 7 post-SCI. In addition, gross anatomical mapping was performed, showing that the lesion area was smaller in Lyz2^{Cre}:H2-Ab1$^{fl/fl}$ mice relative to the control group (Fig. 3B). The results of the MEP and Catwalk analyses were consistent with the BMS scores (Fig. 3C, E). In Motor evoked potential tests, Lyz2^{Cre}:H2-Ab1$^{fl/fl}$ mice has a higher amplitude than other injury groups. In the Catwalk test, Lyz2^{Cre}:H2-Ab1$^{fl/fl}$ mice showed better performance on regularity index and stands(ms) than other injury groups (Fig. 3D, F, G). This means that knocking out *H2-Ab1* in macrophages can promote functional recovery after spinal cord injury.

Knockout of H2-Ab1 in macrophages can alleviate excessive phagocytosis after SCI

To explore the molecular function process of MHC Class II following SCI, IP-MS was conducted, suggesting involvement in phagocytosis and endocytosis (Fig. 4A). Based on recent literature, we found that Arpc2, Cfl1, and Arpc4 proteins play a role through the Fc gamma R-mediated phagocytosis pathway. At the same time, Arpc2, Arpc4, Capza1, Capza2 and Capzb proteins play a role in endocytosis. We performed transmission electron microscopy on spinal cord slices on the 7th day after spinal cord injury (Fig. 4B). The results for the sham group and Cx3cr1^{CreER}:H2-Ab1$^{fl/fl}$ mice are displayed in (Figs. 4A). Results show a reduction in the number of lipid droplets in the macrophages of Lyz2^{Cre}:H2-Ab1$^{fl/fl}$ mice (Fig. 4C). Immunofluorescence double staining for d-MBP (myelin fragments) and Iba1(macrophages and microglia) in samples from the different groups (Fig. 4D)[20, 37], showing that the numbers of myelin-associated Iba1^{+} cells were markedly reduced in Lyz2^{Cre}:H2-Ab1$^{fl/fl}$ relative to H2-Ab1$^{fl/fl}$ mice. Cx3cr1^{CreER}:H2-Ab1$^{fl/fl}$ mice, however, did not show reduced numbers of myelin-associated Iba1^{+} cells (Fig. 4F). Supplementary information (Figs. 4B) also shows the results of the sham group and Cx3cr1^{CreER}:H2-Ab1$^{fl/fl}$ mice. Two lipid labels (Oil Red O and BODIPY) were used to detect lipid droplets in

the damaged area (Fig. 4E, H). It was found that Lyz2^{Cre}:H2-Ab1$^{fl/fl}$ mice had reduced numbers of lipid droplets in the injury center 7 days post-SCI, while Cx3cr1^{CreER}:H2-Ab1$^{fl/fl}$ mice showed no significant change (Fig. 4G, I). Results for the sham group and Cxcr1^{CreER}:H2-Ab1$^{fl/fl}$ mice are also given in Supplementary (Figs. 4C, D). The findings indicate that the formation of foamy macrophages is reduced in Lyz2^{Cre}:H2-Ab1$^{fl/fl}$ mice after SCI.

Knockdown of H2-Ab1 can alleviate excessive phagocytosis and inflammation, thereby reduce the levels of reactive oxygen species (ROS) and apoptosis in neurons in vitro.

To further validate the results of the IP-MS, we used lentivirus to knock down *H2-Ab1* in Raw264.7 cells (a macrophage cell line). We verified the knockdown efficiency and found that sh*H2-Ab1*-2 had the highest knockdown efficiency (Figs. 5A-C). We used this lentivirus for subsequent experiments. The experiment was divided into four groups for in vitro analysis: Raw264.7 + Saline, Raw264.7 + LPS, Raw264.7 + Vector + LPS, and Raw264.7 + sh*H2-Ab1* + LPS. First, we performed phagocytosis assays using spontaneously fluorescent beads of 0.1 μm and 2 μm in size to simulate larger and smaller pathological materials following spinal cord injury. The results showed that phagocytosis was significantly reduced in the Raw264.7 + sh*H2-Ab1* + LPS group compared to the Raw264.7 + LPS and Raw264.7 + Vector + LPS groups (Fig. 5A-B). Next, to investigate whether knockdown of *H2-Ab1* in Raw264.7 cells can reduce intracellular lipid droplets, we performed Oil Red O staining and BODIPY staining. The results showed that knockdown of *H2-Ab1* in Raw264.7 cells can reduce intracellular lipid droplets (Fig. 5C-F). Existing literature reports that excessive lipid droplets in macrophages lead to the formation of foamy macrophages, which in turn promotes the polarization of macrophages toward the M1 phenotype. To investigate the polarization direction of macrophages after *H2-Ab1* knockdown, we performed immunofluorescence staining on these cells (Fig. 5G, I). We quantified the mean fluorescence intensity of iNOS and CD206 in each group. We found that, compared to the Raw264.7 + LPS and Raw264.7 + Vector + LPS groups, the Raw264.7 + sh*H2-Ab1* + LPS group had a lower average fluorescence intensity of iNOS and a higher average fluorescence intensity of CD206 (Fig. 5H, J). At the same time, we assessed the expression of polarization-related proteins (iNOS and CD206) and inflammation-related molecules (TNF-α, IL-1β, and IL-4) using Western blot analysis (Fig. 5K). The results revealed that the Raw264.7 + sh*H2-Ab1* + LPS group exhibited lower expression of iNOS, TNF-α, and IL-1β, and higher expression of CD206 and IL-4 (Fig. 5L). We further conducted indirect co-culture experiments, in which the culture media from each group, collected 24 h after incubation, were added to the corresponding Ht22 cells. Additionally, we investigated the levels of reactive oxygen species (ROS) and apoptosis (Fig. 5M). We quantified the mean fluorescence intensity of DHE and TUNEL staining and found that knockdown of *H2-Ab1* in RAW264.7 cells reduced reactive oxygen species (ROS) levels and apoptosis (Fig. 5N, O).

Knockout of H2-Ab1 in macrophages promotes anti-inflammatory polarization of foamy macrophages

It is well known that phagocytosis of myelin fragments and lipid droplets by macrophages contributes to the inflammatory response [6, 38]. At the same time, M1-type macrophages are often considered to be

detrimental to recovery from SCI [39, 40]. In the preceding text, we have already discovered that MHC Class II molecules are associated with the phagocytosis of macrophages. We would like to know whether MHC Class II molecules promote the polarization of pro-inflammatory macrophages. Compared with H2-Ab1$^{fl/fl}$ mice, lower levels of iNOS and higher levels of CD206 were observed in spinal cord sections on day 7 post-SCI in Lyz2^{Cre}:H2-Ab1$^{fl/fl}$ mice (Fig. 6A-D). We observed co-staining of MHC Class II with iNOS, whereas co-staining of MHC Class II molecules with CD206 was virtually absent. The results of the sham-operated and Cx3cr1^{CreER}:H2-Ab1$^{fl/fl}$ mice are shown in (Figs. 6A, B). qPCR, Western blotting, and flow cytometry showed that Lyz2^{Cre}:H2-Ab1$^{fl/fl}$ mice had higher levels of CD206 and lower iNOS (Fig. 6E-I). The gate information for flow cytometry is provided in the supplementary figures (Figs. 7A-C). Thus, knockout of *H2-Ab1* in macrophages promotes the anti-inflammatory polarization of foamy macrophages.

Knockout of H2-Ab1 in macrophages reduces local inflammation and reactive oxygen species (ROS) following SCI

Our previous study found that *H2-Ab1* knockout in macrophages altered macrophage polarization. Further, we employed qPCR, Western blot, immunofluorescence, and flow cytometry to assess the inflammation levels seven days post-spinal cord injury (SCI). The qPCR results demonstrated that, compared to H2-Ab1$^{fl/fl}$ mice, Il-1β and TNF-α levels were significantly reduced, while IL-4 levels were increased in the spinal cord tissues of Lyz2^{Cre}:H2-Ab1$^{fl/fl}$ mice on the seventh day post-SCI (Fig. 7A). The Western blot results also supported these findings (Fig. 7B-C). We conducted immunofluorescence to detect the levels of CD68 (a marker associated with macrophage inflammation) in mouse spinal cord tissues (Fig. 7D). We found that both the area and intensity of CD68 staining were decreased in Lyz2^{Cre}:H2-Ab1$^{fl/fl}$ mice, indicating lower inflammation in their macrophages (Fig. 7H). To further enhance credibility, we performed flow cytometry on 1-cm-long spinal cord tissue from the injury site seven days post-SCI (Fig. 7E-G). The results showed that Il-1β and TNF-α were significantly decreased, while IL-4 was significantly increased in the macrophages of Lyz2^{Cre}:H2-Ab1$^{fl/fl}$ mice (Fig. 7I-K). This suggests that Lyz2^{Cre}:H2-Ab1$^{fl/fl}$ mice can secrete more anti-inflammatory cytokines and reduce the secretion of pro-inflammatory cytokines, thereby improving the microenvironment of SCI. Additionally, we conducted DHE staining (a dye that can label reactive oxygen species) on frozen sections of spinal cord cross-sections taken from the rostral 2mm segment of the injury site. The results for H2-Ab1$^{fl/fl}$ mice and Lyz2^{Cre}:H2-Ab1$^{fl/fl}$ mice are shown in Fig. 7L, the results for the sham group and Cx3cr1^{CreER}:H2-Ab1$^{fl/fl}$ mice are presented in Figure S8A. We found that the knockout of *H2-Ab1* in macrophages reduced the production of reactive oxygen species (ROS) within neurons (Fig. 7M). This may be due to the decreased secretion of inflammatory cytokines, which alleviates excessive neuronal stress and subsequently reduces the production of ROS within neurons. This suggests that MHC Class II plays a role in macrophages post-SCI, promoting inflammation and exacerbating the production of ROS in neurons.

Knockout of H2-Ab1 in macrophages is associated with tissue repair following SCI

To evaluate the histological recovery associated with conditional knockout of *H2-Ab1* following SCI, 1 cm samples of the injured spinal cord were collected on day 35 following SCI. We first performed TUNEL staining on coronal frozen sections located 2 mm rostral to the spinal cord injury site (Fig. 8A). Statistical analysis revealed that the knockout of *H2-Ab1* in macrophages can significantly reduce the occurrence of apoptosis (Fig. 8D). It was observed that the lesion area was smaller in $Lyz2^{Cre}$:$H2\text{-}Ab1^{fl/fl}$ mice relative to the controls, as shown by HE staining (Fig. 8B, E). Additionally, the Nissl staining results indicated that there were more surviving neurons in $Lyz2^{Cre}$:$H2\text{-}Ab1^{fl/fl}$ mice (Fig. 8C, G) [41]. This may be related to the reduction in apoptosis. However, the lesion area and neuron survival in $Cx3cr1^{CreER}$:$H2\text{-}Ab1^{fl/fl}$ mice were equivalent to those in $H2\text{-}Ab1^{fl/fl}$ mice. It is thus suggested that knockout of *H2-Ab1* in macrophages, rather than microglia, may promote tissue repair and morphological recovery. Immunofluorescence staining was conducted, labeling neurofilaments with NF200 and glial scars with GFAP (Fig. 8F) [42, 43]. This showed that the neurofilament density in $Lyz2^{Cre}$:$H2\text{-}Ab1^{fl/fl}$ mice was markedly greater than that in the other groups, while glial scars were smaller (Fig. 8H, J). Additionally, we also stained for fibronectin produced by fibroblasts (Fig. 8I). We observed that fibrous scars often locate within and fill the glial scars. $Lyz2^{Cre}$:$H2\text{-}Ab1^{fl/fl}$ mice mice exhibited the smallest fibrous scars (Fig. 8K). However, $Cx3cr1^{CreER}$:$H2\text{-}Ab1^{fl/fl}$ mice did not show improvement in reducing fibrous scars. Finally, we stained for 5-HT nerves (Figs. 9A). Results demonstrated better recovery in $Lyz2^{Cre}$:$H2\text{-}Ab1^{fl/fl}$ mice (Figs. 9B). Thus, knockout of *H2-Ab1* in macrophages is associated with morphological improvements after spinal cord injury.

Discussion

Spinal cord injury is a central nervous system disorder with no effective treatment available, often resulting in severe physiological and psychological trauma. In recent years, an increasing number of studies have shown that macrophages play an important role in spinal cord injury, often exhibiting a "double-edged sword" effect [39, 44, 45]. For example, the glial scars formed by macrophages have a positive role in limiting the injury area, but they may also become a negative factor that hinders neuronal regeneration. The phagocytic activity of macrophages is similar. Moderate phagocytosis can clear necrotic cells, apoptotic cells, and cellular debris following spinal cord injury, which helps improve the condition. However, excessive phagocytosis leads to the transformation of macrophages into foamy macrophages, significantly increasing the secretion of inflammatory factors, thereby exacerbating the inflammatory response, and worsening the microenvironment of the injury. In this study, we demonstrated that knocking out *H2-Ab1* in macrophages, rather than in microglia, could alleviate excessive phagocytosis, thereby improving the spinal cord injury microenvironment, reducing neuronal apoptosis, and ultimately promoting recovery from spinal cord injury (Graphical abstract).

MHC Class II molecules consist of two chains: an α chain and a β chain, with the H2-Ab1 gene specifically encoding a subunit of the β chain. When *H2-Ab1* is knocked out, it affects the assembly of MHC Class II molecules. MHC Class II molecules have been extensively studied in diseases such as Alzheimer's disease and cancer, where they play significant roles, such as in cell activation and

differentiation, and antigen presentation. In this study, we first linked *H2-Ab1* with the phagocytosis of macrophages in spinal cord injury, further enhancing our understanding of the role of the *H2-Ab1* and its potential mechanisms in the nervous system

Results showed that the expression level of MHC Class II molecules peaked on the seventh day after spinal cord injury. However, both microglia and macrophages express MHC Class II after spinal cord injury, and because they share similar surface markers, they are difficult to distinguish. To address this, we bred $Cx3cr1^{CreER}$:R26-TdTomato and $Lyz2^{Cre}$:R26-TdTomato reporter mice. This study provides the first report that MHC Class II molecules are primarily expressed in macrophages following spinal cord injury. In addition, the expression of MHC Class II following spinal cord injury shows regional differences. MHC Class II molecules are most prominently expressed at the injury boundary, moderately expressed at the injury center, and almost undetectable in regions distant from the injury. This distribution closely mirrors the infiltration pattern of macrophages in spinal cord injury, further supporting the idea that *H2-Ab1* functions through infiltrating macrophages.

The results showed that knocking out *H2-Ab1* in macrophages, rather than in microglia, improved spinal cord injury both functionally and histologically. Through immunoprecipitation mass spectrometry (IP-MS) and transcriptomic analysis, we found that *H2-Ab1* may be involved in phagocytosis. In this study, we used myelin debris and lipid droplet counts in macrophages as indicators of phagocytic activation to assess phagocytosis following spinal cord injury. Myelin debris clearance after spinal cord injury is primarily carried out through macrophage phagocytosis[46]. Recent studies have revealed that microglial cells are primarily located at the injury margins and in undamaged areas, and their efficiency in myelin debris phagocytosis is much lower than that of macrophages [6, 46]. In different disease models, the effect of phagocytosis on macrophage polarization in vivo remains controversial. In multiple sclerosis and atherosclerosis, myelin-laden macrophages express various anti-inflammatory molecules[47, 48]. In contrast, in spinal cord injury, the formation of foamy macrophages is associated with the upregulation of pro-inflammatory polarization[6, 46]. Additionally, results from in vitro stimulation of macrophages with myelin debris also present conflicting findings. Some studies report that phagocytosis induces the release of inflammatory cytokines [49], while others show that macrophages that undergo phagocytosis express anti-inflammatory mediators in response to pro-inflammatory stimuli, and the molecular mechanisms behind these contradictory findings remain unclear [39]. In our study, excessive phagocytosis promoted the formation of foamy macrophages and led to pro-inflammatory polarization of macrophages following spinal cord injury. Furthermore, we found that knocking out *H2-Ab1* in macrophages significantly alleviated excessive phagocytosis, reduced inflammation, decreased ROS production, and improved neuronal survival. This finding further confirms the negative impact of excessive phagocytosis on spinal cord injury and provides new insights for potential treatments of spinal cord injury.

Conclusion

The results of this study indicate that knockout of *H2-Ab1* in macrophages, rather than microglia, inhibited phagocytosis, altered macrophage polarization, and improved the inflammatory microenvironment. This further reduced the scar area and neuronal apoptosis, ultimately improving spinal cord injury. These results provide a theoretical foundation and suggest new research directions for gene editing in macrophages to ameliorate spinal cord injury, offering potential novel targets for clinical treatment.

Declarations

Ethics Approval and Consent to Participate

This study was approved by the Ethics Committee of Sun Yat-sen University, Guangzhou, China (Approval number: 2021-7071; Ethics application number: 2023003115).

Consent for Publication

All authors consent to the publication of this manuscript.

Availability of Data and Materials

The datasets generated and/or analyzed during this study are available from the corresponding author upon reasonable request.

Competing Interests

The authors declare that they have no competing interests.

Funding

This research was supported by the National Natural Science Foundation of China (Grant numbers: U22A20297, 82172433, 82102642, 823B2060, 82604702) and the Key Research and Development Program of Guangzhou (Grant number: 202206060003). Postdoctoral Fellowship Program of China Postdoctoral Science Foundation (GZB20240904) The China Postdoctoral Science Foundation (2024M763769). Guangdong Basic and Applied Basic Research Foundation(2024A1515013070, 2025A1515012371).

Authors' Contributions

Conceptualization, TLZ, YK, BL and LMR; Methodology, TLZ, LMR, HJZ and SYY; Investigation, TLZ, YY, and BL; Formal Analysis, TLZ, YK; Writing, TLZ, YK, SYY and LMR; Funding Acquisition, LMR and SYY. All authors reviewed and approved the manuscript.

Acknowledgements

The graphical abstract was created using BioRender.com.

References

1. Collaborators GBDN: Global, regional, and national burden of neurological disorders, 1990–2016: a systematic analysis for the Global Burden of Disease Study 2016. *Lancet Neurol* 2019, 18(5):459–480.
2. Alizadeh A, Dyck SM, Karimi-Abdolrezaee S: Traumatic Spinal Cord Injury: An Overview of Pathophysiology, Models and Acute Injury Mechanisms. *Front Neurol* 2019, 10:282.
3. Pang QM, Chen SY, Fu SP, Zhou H, Zhang Q, Ao J, Luo XP, Zhang T: Regulatory Role of Mesenchymal Stem Cells on Secondary Inflammation in Spinal Cord Injury. *J Inflamm Res* 2022, 15:573–593.
4. Ahuja CS, Martin AR, Fehlings M: Recent advances in managing a spinal cord injury secondary to trauma. *F1000Res* 2016, 5.
5. Milich LM, Ryan CB, Lee JK: The origin, fate, and contribution of macrophages to spinal cord injury pathology. *Acta Neuropathol* 2019, 137(5):785–797.
6. Van Broeckhoven J, Sommer D, Dooley D, Hendrix S, Franssen A: Macrophage phagocytosis after spinal cord injury: when friends become foes. *Brain* 2021, 144(10):2933–2945.
7. Ageeva T, Rizvanov A, Mukhamedshina Y: NF-kappaB and JAK/STAT Signaling Pathways as Crucial Regulators of Neuroinflammation and Astrocyte Modulation in Spinal Cord Injury. *Cells* 2024, 13(7).
8. Fang YP, Qin ZH, Zhang Y, Ning B: Implications of microglial heterogeneity in spinal cord injury progression and therapy. *Exp Neurol* 2023, 359:114239.
9. Zhai C, Wang Z, Cai J, Fang L, Li X, Jiang K, Shen Y, Wang Y, Xu X, Liu W *et al*: Repeated trans-spinal magnetic stimulation promotes microglial phagocytosis of myelin debris after spinal cord injury through LRP-1. *Exp Neurol* 2024, 379:114844.
10. Kopper TJ, Gensel JC: Myelin as an inflammatory mediator: Myelin interactions with complement, macrophages, and microglia in spinal cord injury. *J Neurosci Res* 2018, 96(6):969–977.
11. David S, Kroner A: Repertoire of microglial and macrophage responses after spinal cord injury. *Nat Rev Neurosci* 2011, 12(7):388–399.
12. Ma D, Shen H, Chen F, Liu W, Zhao Y, Xiao Z, Wu X, Chen B, Lu J, Shao D *et al*: Inflammatory Microenvironment-Responsive Nanomaterials Promote Spinal Cord Injury Repair by Targeting IRF5. *Adv Healthc Mater* 2022, 11(23):e2201319.
13. Ryan CB, Choi JS, Kang B, Herr S, Pereira C, Moraes CT, Al-Ali H, Lee JK: PI3K signaling promotes formation of lipid-laden foamy macrophages at the spinal cord injury site. *Neurobiol Dis* 2024, 190:106370.
14. Nakayama M, Takeda K, Kawano M, Takai T, Ishii N, Ogasawara K: Natural killer (NK)-dendritic cell interactions generate MHC class II-dressed NK cells that regulate CD4 + T cells. *Proc Natl Acad Sci U S A* 2011, 108(45):18360–18365.
15. MARTIN BAUMGART VM: Differential expression of major histocompatibility complex class II genes on murine macrophages associated with T cell cytokine profile and protective/suppressive effects. *Proc Natl Acad Sci USA* 1998, 95, pp. 6936–6940, June 1998.

16. Zhou Y, Luo Z, Liao C, Cao R, Hussain Z, Wang J, Zhou Y, Chen T, Sun J, Huang Z *et al*: MHC class II in renal tubules plays an essential role in renal fibrosis. *Cell Mol Immunol* 2021, 18(11):2530–2540.
17. Jamwal DR, Laubitz D, Harrison CA, Figliuolo da Paz V, Cox CM, Wong R, Midura-Kiela M, Gurney MA, Besselsen DG, Setty P *et al*: Intestinal Epithelial Expression of MHCII Determines Severity of Chemical, T-Cell-Induced, and Infectious Colitis in Mice. *Gastroenterology* 2020, 159(4):1342–1356 e1346.
18. Munz C: Autophagy Beyond Intracellular MHC Class II Antigen Presentation. *Trends Immunol* 2016, 37(11):755–763.
19. Francos-Quijorna I, Sanchez-Petidier M, Burnside ER, Badea SR, Torres-Espin A, Marshall L, de Winter F, Verhaagen J, Moreno-Manzano V, Bradbury EJ: Chondroitin sulfate proteoglycans prevent immune cell phenotypic conversion and inflammation resolution via TLR4 in rodent models of spinal cord injury. *Nat Commun* 2022, 13(1):2933.
20. Gao H, Di J, Clausen BH, Wang N, Zhu X, Zhao T, Chang Y, Pang M, Yang Y, He R *et al*: Distinct myeloid population phenotypes dependent on TREM2 expression levels shape the pathology of traumatic versus demyelinating CNS disorders. *Cell Rep* 2023, 42(6):112629.
21. Kopper TJ, Zhang B, Bailey WM, Bethel KE, Gensel JC: The effects of myelin on macrophage activation are phenotypic specific via cPLA(2) in the context of spinal cord injury inflammation. *Sci Rep* 2021, 11(1):6341.
22. Gao P, Yi J, Chen W, Gu J, Miao S, Wang X, Huang Y, Jiang T, Li Q, Zhou W *et al*: Pericyte-derived exosomal miR-210 improves mitochondrial function and inhibits lipid peroxidation in vascular endothelial cells after traumatic spinal cord injury by activating JAK1/STAT3 signaling pathway. *J Nanobiotechnology* 2023, 21(1):452.
23. Zhang W, Lu J, Wang Y, Sun P, Gao T, Xu N, Zhang Y, Xie W: Canagliflozin Attenuates Lipotoxicity in Cardiomyocytes by Inhibiting Inflammation and Ferroptosis through Activating AMPK Pathway. *Int J Mol Sci* 2023, 24(1).
24. Sun X, Liu H, Tan Z, Hou Y, Pang M, Chen S, Xiao L, Yuan Q, Liu B, Rong L *et al*: Remodeling Microenvironment for Endogenous Repair through Precise Modulation of Chondroitin Sulfate Proteoglycans Following Spinal Cord Injury. *Small* 2023, 19(6):e2205012.
25. Huang X, Fan J, Li L, Liu H, Wu R, Wu Y, Wei L, Mao H, Lal A, Xi P *et al*: Fast, long-term, super-resolution imaging with Hessian structured illumination microscopy. *Nat Biotechnol* 2018, 36(5):451–459.
26. Milich LM, Choi JS, Ryan C, Cerqueira SR, Benavides S, Yahn SL, Tsoulfas P, Lee JK: Single-cell analysis of the cellular heterogeneity and interactions in the injured mouse spinal cord. *J Exp Med* 2021, 218(8).
27. Li C, Wu Z, Zhou L, Shao J, Hu X, Xu W, Ren Y, Zhu X, Ge W, Zhang K *et al*: Temporal and spatial cellular and molecular pathological alterations with single-cell resolution in the adult spinal cord after injury. *Signal Transduct Target Ther* 2022, 7(1):65.

28. Zhang Q, Yu B, Zhang Y, Tian Y, Yang S, Chen Y, Wu H: Combination of single-cell and bulk RNA seq reveals the immune infiltration landscape and targeted therapeutic drugs in spinal cord injury. *Front Immunol* 2023, 14:1068359.
29. Aran D, Looney AP, Liu L, Wu E, Fong V, Hsu A, Chak S, Naikawadi RP, Wolters PJ, Abate AR *et al*: Reference-based analysis of lung single-cell sequencing reveals a transitional profibrotic macrophage. *Nat Immunol* 2019, 20(2):163–172.
30. D. MICHELE BASSO LCF: Basso Mouse Scale for Locomotion Detects Differences in Recovery after Spinal Cord Injury in Five Common Mouse Strains. *JOURNAL OF NEUROTRAUMA* 2006.
31. Rong Y, Fan J, Ji C, Wang Z, Ge X, Wang J, Ye W, Yin G, Cai W, Liu W: USP11 regulates autophagy-dependent ferroptosis after spinal cord ischemia-reperfusion injury by deubiquitinating Beclin 1. *Cell Death Differ* 2022, 29(6):1164–1175.
32. Li Q, Zhao Y, Guo H, Li Q, Yan C, Li Y, He S, Wang N, Wang Q: Impaired lipophagy induced-microglial lipid droplets accumulation contributes to the buildup of TREM1 in diabetes-associated cognitive impairment. *Autophagy* 2023, 19(10):2639–2656.
33. Zhao SJ, Kong FQ, Cai W, Xu T, Zhou ZM, Wang ZB, Xu AD, Yang YQ, Chen J, Tang PY *et al*: GIT1 contributes to autophagy in osteoclast through disruption of the binding of Beclin1 and Bcl2 under starvation condition. *Cell Death Dis* 2018, 9(12):1195.
34. Griffin JM, Bradke F: Therapeutic repair for spinal cord injury: combinatory approaches to address a multifaceted problem. *EMBO Mol Med* 2020, 12(3):e11505.
35. Ma D, Zhao Y, Huang L, Xiao Z, Chen B, Shi Y, Shen H, Dai J: A novel hydrogel-based treatment for complete transection spinal cord injury repair is driven by microglia/macrophages repopulation. *Biomaterials* 2020, 237:119830.
36. Hashimoto K, Joshi SK, Koni PA: A conditional null allele of the major histocompatibility IA-beta chain gene. *Genesis* 2002, 32(2):152–153.
37. Zhu K, Sun J, Kang Z, Zou Z, Wu G, Wang J: Electroacupuncture Promotes Remyelination after Cuprizone Treatment by Enhancing Myelin Debris Clearance. *Front Neurosci* 2016, 10:613.
38. Schilperoort M, Ngai D, Sukka SR, Avrampou K, Shi H, Tabas I: The role of efferocytosis-fueled macrophage metabolism in the resolution of inflammation. *Immunol Rev* 2023, 319(1):65–80.
39. Kroner A, Greenhalgh AD, Zarruk JG, Passos Dos Santos R, Gaestel M, David S: TNF and increased intracellular iron alter macrophage polarization to a detrimental M1 phenotype in the injured spinal cord. *Neuron* 2014, 83(5):1098–1116.
40. Xu GY, Xu S, Zhang YX, Yu ZY, Zou F, Ma XS, Xia XL, Zhang WJ, Jiang JY, Song J: Cell-Free Extracts from Human Fat Tissue with a Hyaluronan-Based Hydrogel Attenuate Inflammation in a Spinal Cord Injury Model through M2 Microglia/Microphage Polarization. *Small* 2022, 18(17):e2107838.
41. Yao S, Pang M, Wang Y, Wang X, Lin Y, Lv Y, Xie Z, Hou J, Du C, Qiu Y *et al*: Mesenchymal stem cell attenuates spinal cord injury by inhibiting mitochondrial quality control-associated neuronal ferroptosis. *Redox Biol* 2023, 67:102871.

42. Li X, Zhang C, Haggerty AE, Yan J, Lan M, Seu M, Yang M, Marlow MM, Maldonado-Lasuncion I, Cho B *et al*: The effect of a nanofiber-hydrogel composite on neural tissue repair and regeneration in the contused spinal cord. *Biomaterials* 2020, 245:119978.
43. Raffaele S, Thougaard E, Laursen CCH, Gao H, Andersen KM, Nielsen PV, Orti-Casan N, Blichfeldt-Eckhardt M, Koch S, Deb-Chatterji M *et al*: Microglial TNFR2 signaling regulates the inflammatory response after CNS injury in a sex-specific fashion. *Brain Behav Immun* 2024, 116:269–285.
44. Huang F, Lu X, Kuai L, Ru Y, Jiang J, Song J, Chen S, Mao L, Li Y, Li B *et al*: Dual-Site Biomimetic Cu/Zn-MOF for Atopic Dermatitis Catalytic Therapy via Suppressing FcgammaR-Mediated Phagocytosis. *J Am Chem Soc* 2024, 146(5):3186–3199.
45. St-Pierre MK, Gonzalez Ibanez F, Kroner A, Tremblay ME: Microglia/macrophages are ultrastructurally altered by their proximity to spinal cord injury in adult female mice. *J Neuroinflammation* 2023, 20(1):273.
46. Wang X, Cao K, Sun X, Chen Y, Duan Z, Sun L, Guo L, Bai P, Sun D, Fan J *et al*: Macrophages in spinal cord injury: phenotypic and functional change from exposure to myelin debris. *Glia* 2015, 63(4):635–651.
47. Spann NJ, Garmire LX, McDonald JG, Myers DS, Milne SB, Shibata N, Reichart D, Fox JN, Shaked I, Heudobler D *et al*: Regulated accumulation of desmosterol integrates macrophage lipid metabolism and inflammatory responses. *Cell* 2012, 151(1):138–152.
48. Boven LA, Van Meurs M, Van Zwam M, Wierenga-Wolf A, Hintzen RQ, Boot RG, Aerts JM, Amor S, Nieuwenhuis EE, Laman JD: Myelin-laden macrophages are anti-inflammatory, consistent with foam cells in multiple sclerosis. *Brain* 2006, 129(Pt 2):517–526.
49. van der Laan LJ, Ruuls SR, Weber KS, Lodder IJ, Dopp EA, Dijkstra CD: Macrophage phagocytosis of myelin in vitro determined by flow cytometry: phagocytosis is mediated by CR3 and induces production of tumor necrosis factor-alpha and nitric oxide. *J Neuroimmunol* 1996, 70(2):145–152.

Figures

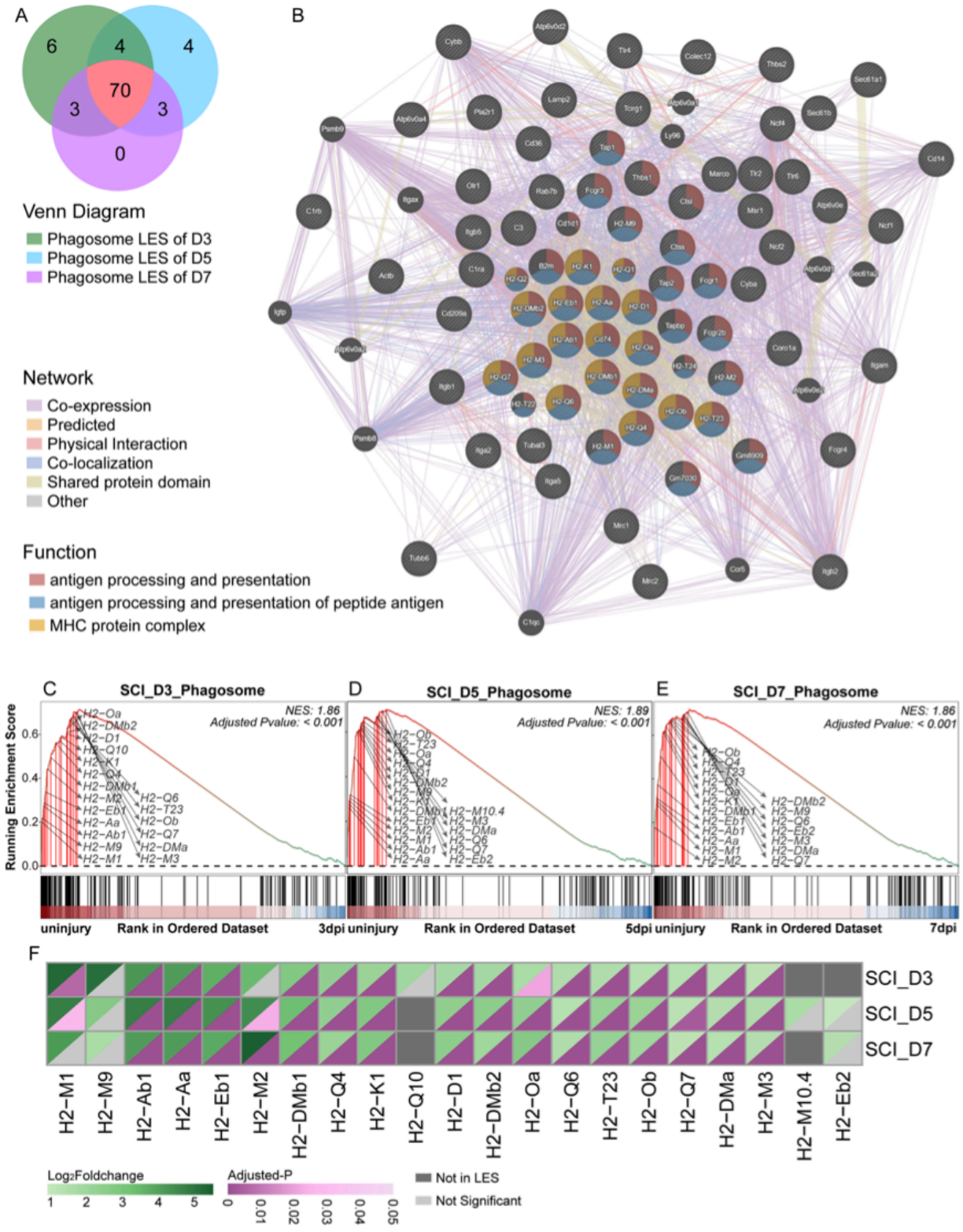


Figure 1

H2-Ab1 is a core gene in the phagosome pathway after SCI.

A Venn diagram of the phagosome leading edge subset (LES) at 3, 5, and 7 days after SCI. **B** Protein-protein interaction network for the intersection genes of phagosome LES at 3, 5, and 7 days after SCI. **C-**

EH2 family genes in phagosome LES at three time points, identified by GSEA. **F**Heatmap of H2 family genes in phagosome LES at 3, 5, and 7 days after SCI.

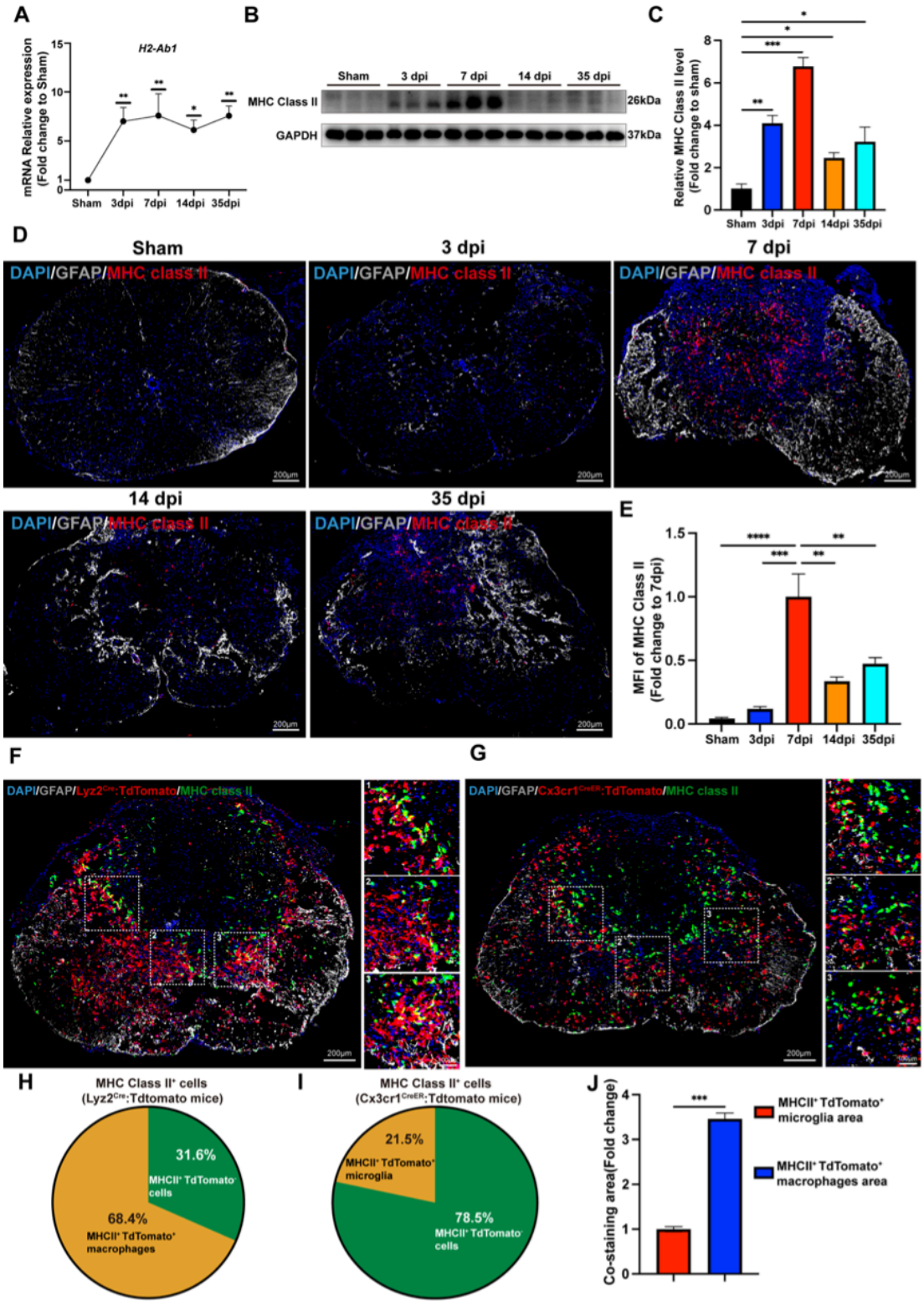


Figure 2

MHC Class II is up-regulated and primarily co-localized with macrophages at 7days after SCI.

A qPCR analysis of *H2-Ab1* levels in mice from sham group and the spinal cord injury (SCI) groups at 3-, 7-, 14-, and 35-days post-injury. n=3. **B-C** Western blotting (B) and quantification (C) of MHC Class II levels in sham group and the spinal cord injury (SCI) groups at 3-, 7-, 14-, and 35-days post-injury, with GAPDH as the loading control. Conditions were the same for all gels. **D-E** Representative immunofluorescence images (D) and quantification (E) of MHC Class II at each timepoint after SCI. Scale bar: 200 μm. **F** Representative immunofluorescence images of MHC Class II in $Lyz2^{Cre}$:R26-TdTomato mice at 7 days after SCI. Scale bar: 200 μm. Three enlarged regions of the randomly selected damage boundary for each sample. **G** Representative immunofluorescence images of MHC Class II in $Cx3cr1^{CreER}$:R26-TdTomato mice at 7 days after SCI. Scale bar: 200 μm. Three enlarged regions of the randomly selected damage boundary for each sample. **H** The proportion of macrophages expressing MHC Class II among MHC Class II^+ cells. **I** The proportion of microglia expressing MHC Class II among MHC Class II^+ cells. **J** Area ratio of MHC Class II^+ $TdTomato^+$ microglia and MHC Class II^+ $TdTomato^+$ macrophages. Data are mean ± SEM. *P < 0.05, **P < 0.01, ***P < 0.001, ****P < 0.0001.

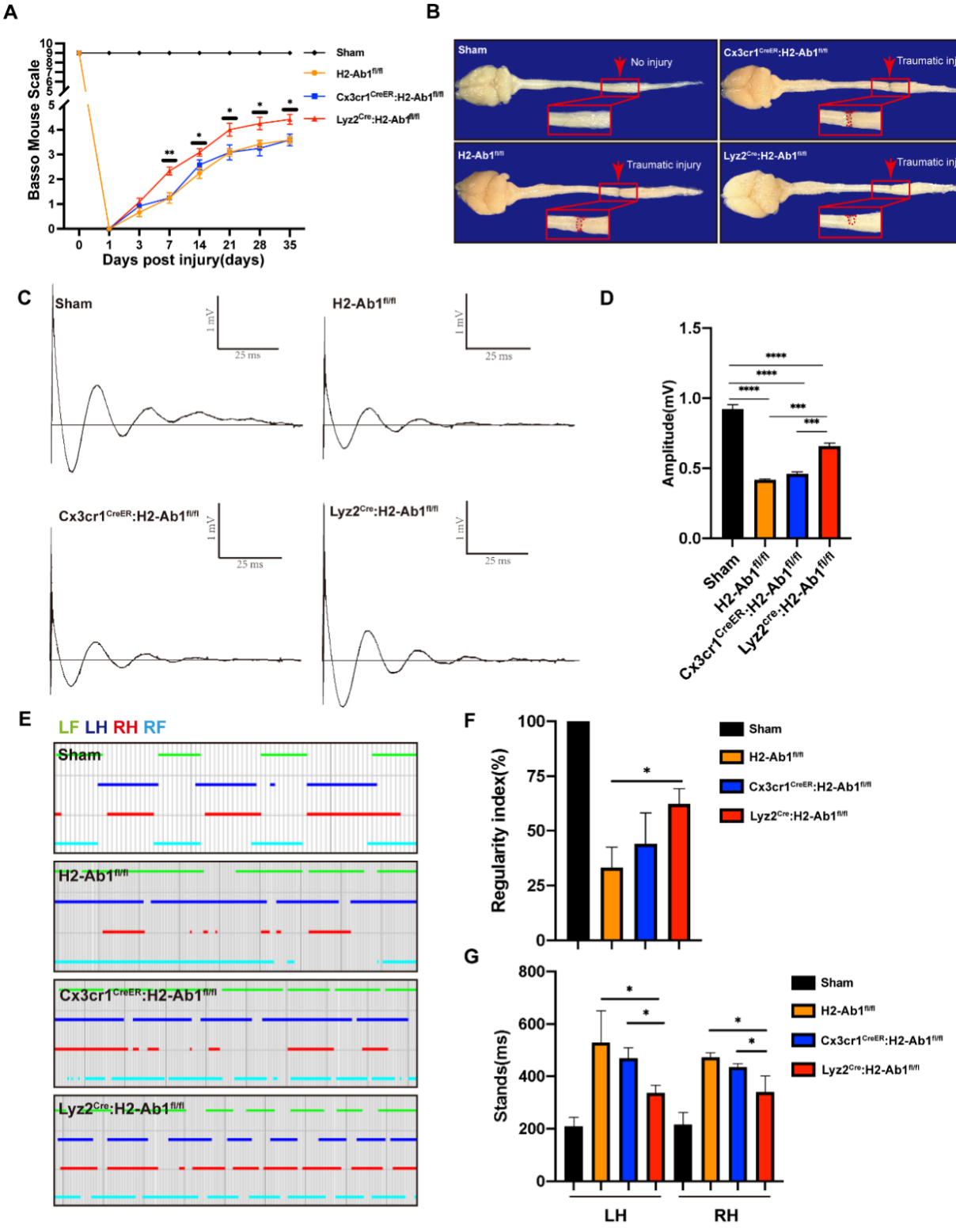


Figure 3

***H2-Ab1* knockout in macrophages promotes recovery of motor function after SCI.**

A Measurement of BMS scores on day 0, 1, 3, 7, 14, 21, 28 and 35 post injury in sham, H2-Ab1$^{fl/fl}$, Cx3cr1^{CreER}:H2-Ab1$^{fl/fl}$, and Lyz2^{Cre}:H2-Ab1$^{fl/fl}$ groups. n=6. **B** Representative gross anatomical maps showing the lesion core at day 35 following SCI. Scale bar: 1 cm. **C** Representative diagrams of MEP

measurements on day 35 following SCI in the sham, H2-Ab1$^{fl/fl}$, Cx3cr1^{CreER}:H2-Ab1$^{fl/fl}$, and Lyz2^{Cre}:H2-Ab1$^{fl/fl}$ groups. **D** Quantitative analysis of the amplitude of the first peak (mV) in (C). **E** Representative images of mouse footprints on day 35 following SCI. n=5. **F** Statistical analysis of regular index (RI) (%) according to (E) **G** Statistical analysis of standing (s) for both hindlimbs according to gragh E. Data are mean ± SEM. *P < 0.05, **P < 0.01, ***P < 0.001, ****P < 0.0001.

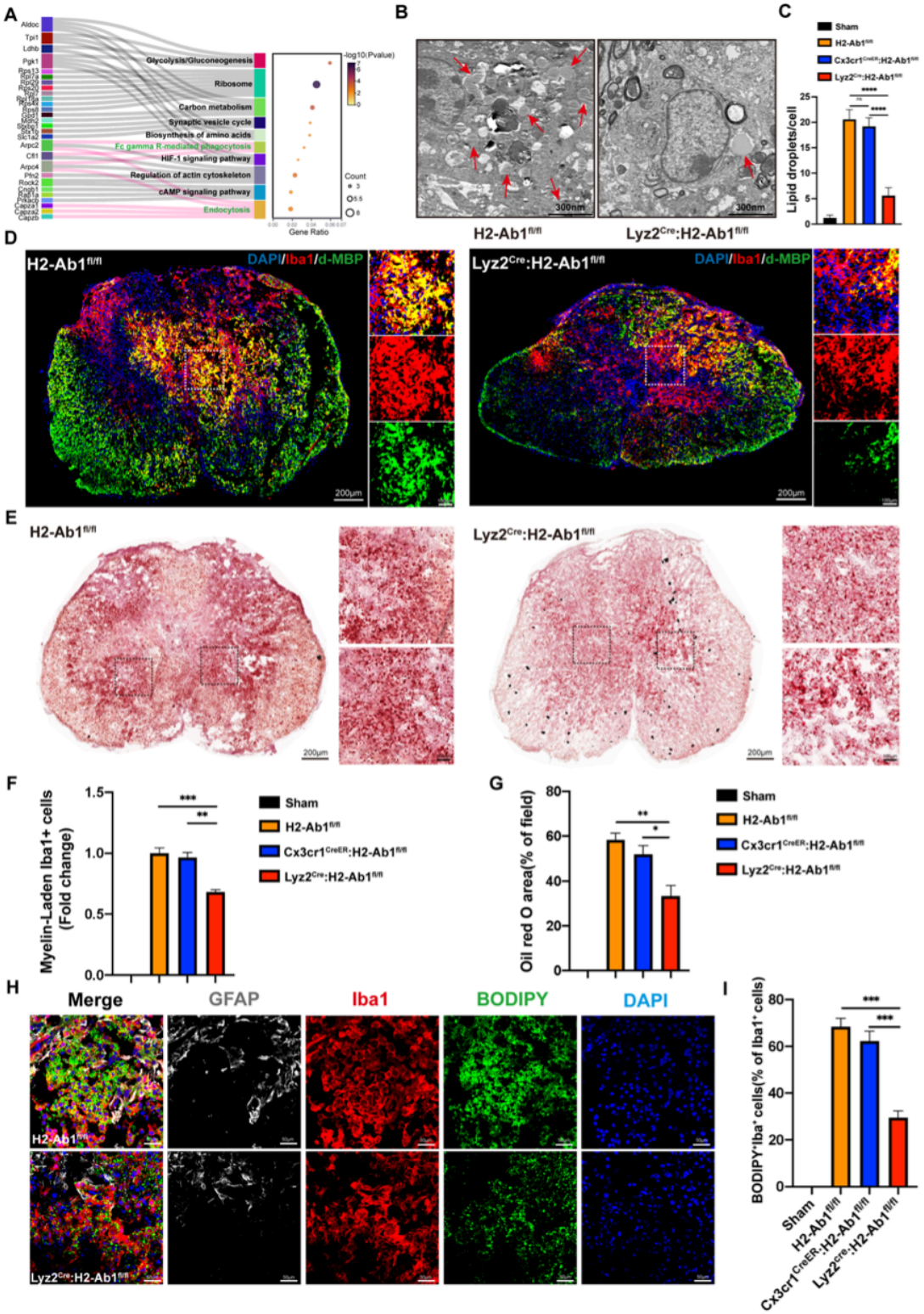


Figure 4

A IP-MS identification of proteins binding to MHC Class II following SCI and associated KEGG pathways. **B** Transmission electron micrographs of foamy macrophages in the lesion sites of H2-Ab1$^{fl/fl}$ and Lyz2^{Cre}:H2-Ab1$^{fl/fl}$ mice on day 7 after SCI. The red arrow indicates lipid droplets in foamy macrophages. **C** Quantification of the number of lipid droplets per macrophage. n=5. **D** Representative immunostaining on day 7 following SCI in the H2-Ab1$^{fl/fl}$ and Lyz2^{Cre}:H2-Ab1$^{fl/fl}$ groups; microglia and macrophages indicated by Iba1 and myelin debris indicated by d-MBP. **E** Representative images showing Oil Red O staining of the lesion sites on day 7 following SCI in the H2-Ab1$^{fl/fl}$ and Lyz2^{Cre}:H2-Ab1$^{fl/fl}$ groups. **F** Quantification of Iba1^{+} myelin-laden macrophages/microglia in the lesion site on day 7 following SCI. n=5. **G** Quantification of Oil Red O staining area in the H2-Ab1$^{fl/fl}$ and Lyz2^{Cre}:H2-Ab1$^{fl/fl}$ groups. n=5. **H** Representative immunostaining on day 7 following SCI in the H2-Ab1$^{fl/fl}$ and Lyz2^{Cre}:H2-Ab1$^{fl/fl}$ groups; macrophages and microglia indicated by Iba1 and lipid droplets by BODIPY. **I** Quantification of BODIPY-stained cells in the H2-Ab1$^{fl/fl}$ and Lyz2^{Cre}:H2-Ab1$^{fl/fl}$ groups. Data are mean ± SEM. *P < 0.05, **P < 0.01, ***P < 0.001, ****P < 0.0001.

***H2-Ab1* knockout in macrophages reduces the formation of foamy macrophages.**

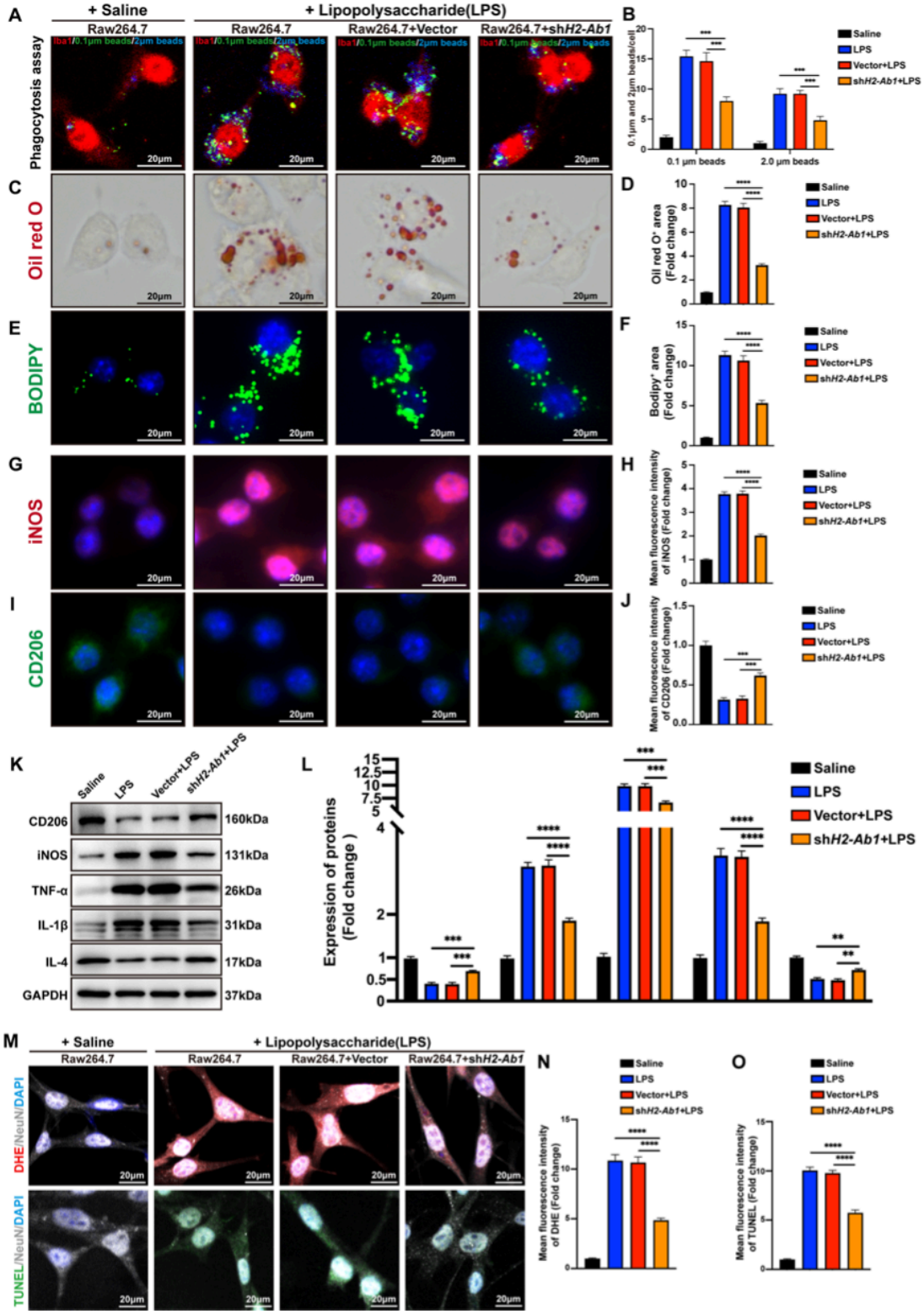


Figure 5

Knockdown of H2-Ab1 can alleviate excessive phagocytosis and inflammation, thereby reduce the levels of reactive oxygen species (ROS) and apoptosis in neurons in vitro.

A Representative Iba1 immunostaining pictures of Raw264.7 cells phagocytosing fluoresent beads with different sizes from different groups. Green dots represent 0.1μm autoflurecent beads. Blue dots

represent 2 μm autoflurecent beads. Scale bar, 20 μm. **B**Quantification of phagocytosed bead numbers in Raw264.7 cells from different groups. n=5. **C** Representative images showing Oil Red O staining of Raw264.7 cells from different groups. **D** Quantification of Oil Red O staining area from different groups. n=5. **E** Representative images of BODIPY staining of Raw264.7 cells from different groups. **F** Quantification of Oil Red O staining area from different groups. n=5. **G** Representative immunostaining of iNOS of Raw264.7 cells from different groups. **H**Quantification of the mean fluorescence intensity of iNOS in representative images from different groups. n=5. **I** Representative immunostaining of CD206 of Raw264.7 cells from different groups. **J** Quantification of the mean fluorescence intensity of CD206 in representative images from different groups. n=5. **K** Western blotting of iNOS, CD206, TNF-α, IL-1β and IL-4 in Raw264.7 cells from different groups, with GAPDH as loading control. **L**Quantification of iNOS, CD206, TNF-α, IL-1β and IL-4 expression by Western blot in different groups. n=5. **M** Representative images of DHE and TUNEL staining in Ht22 cells from different groups. **N** Quantification of the mean fluorescence intensity of DHE in representative images from different groups. n=5. O Quantification of the mean fluorescence intensity of TUNEL in representative images from different groups. n=5. Data are mean ± SEM. *P < 0.05, **P < 0.01, ***P < 0.001, ****P < 0.0001.

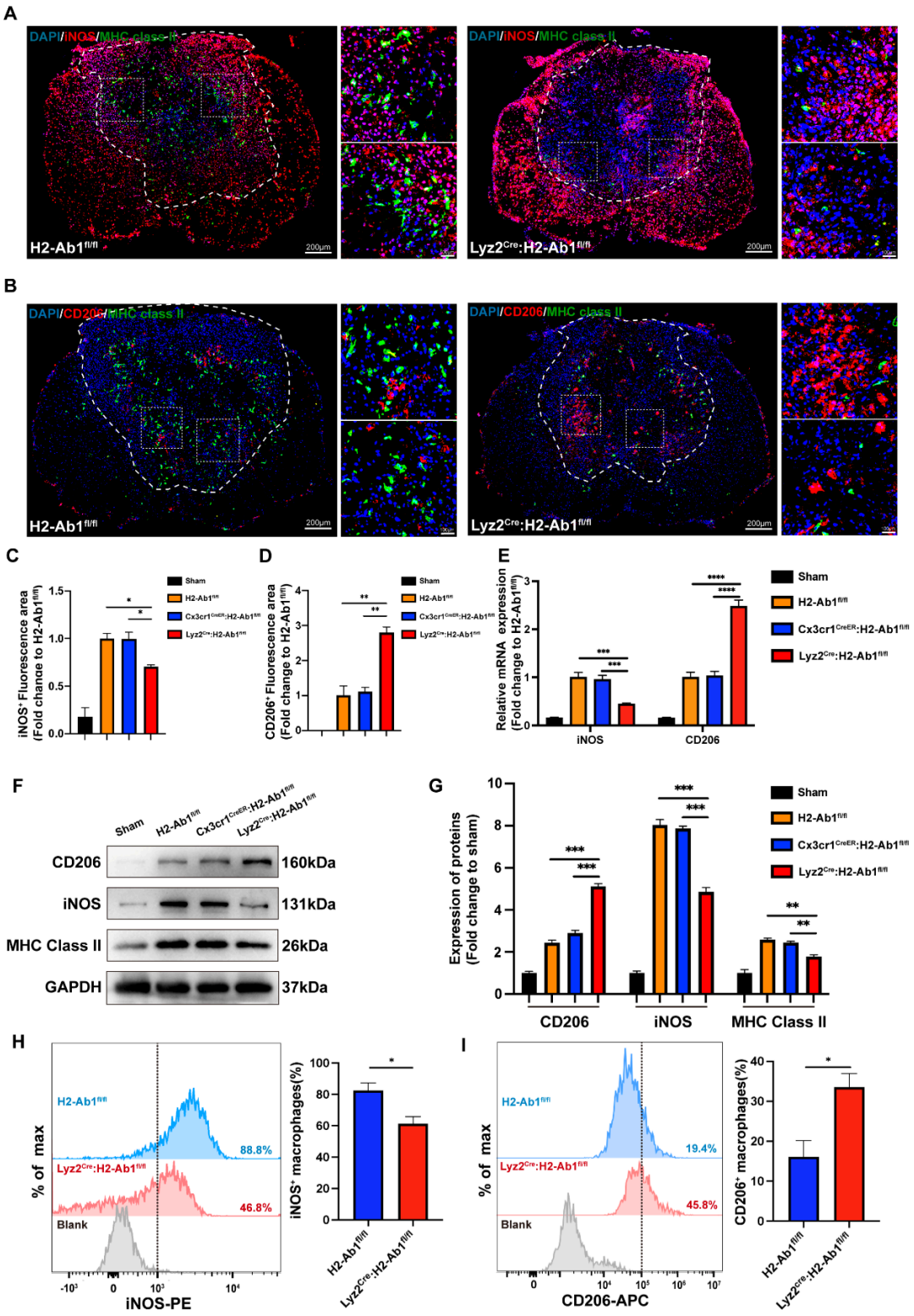


Figure 6

H2-Ab1 knockout in macrophages alters macrophage phenotype from M1 to M2.

A-B Representative immunostaining at day 7 after SCI in the H2-Ab1$^{fl/fl}$ and Lyz2^{Cre}:H2-Ab1$^{fl/fl}$ mice. M1 macrophages indicated by iNOS; M2 macrophages indicated by CD206. **C-D** The fluorescent area within the injury region (dashed line) for CD206 and iNOS was quantified in each group. (Representative

immunostaining for sham and Cx3cr1^{CreER}:H2-Ab1$^{fl/fl}$ showed in Figs.5). **E** qPCR analysis of CD206 and iNOS levels from different groups. **F** Western blotting of MHC Class II, iNOS and CD206 from different groups, with GAPDH as loading control. **G** Quantification of MHC Class II, iNOS and CD206 expression by Western blot in different groups. n=5. **H** Flow cytometry and quantification of percentages of iNOS^{+} macrophages at day 7 following SCI in H2-Ab1$^{fl/fl}$ and Lyz2^{Cre}:H2-Ab1$^{fl/fl}$ mice. n=5. **I** Flow cytometry and quantification of percentages of CD206^{+} macrophages at day 7 following SCI in H2-Ab1$^{fl/fl}$ and Lyz2^{Cre}:H2-Ab1$^{fl/fl}$ mice. n=5. Data are mean ± SEM. *P < 0.05, **P < 0.01, ***P < 0.001, ****P < 0.0001.

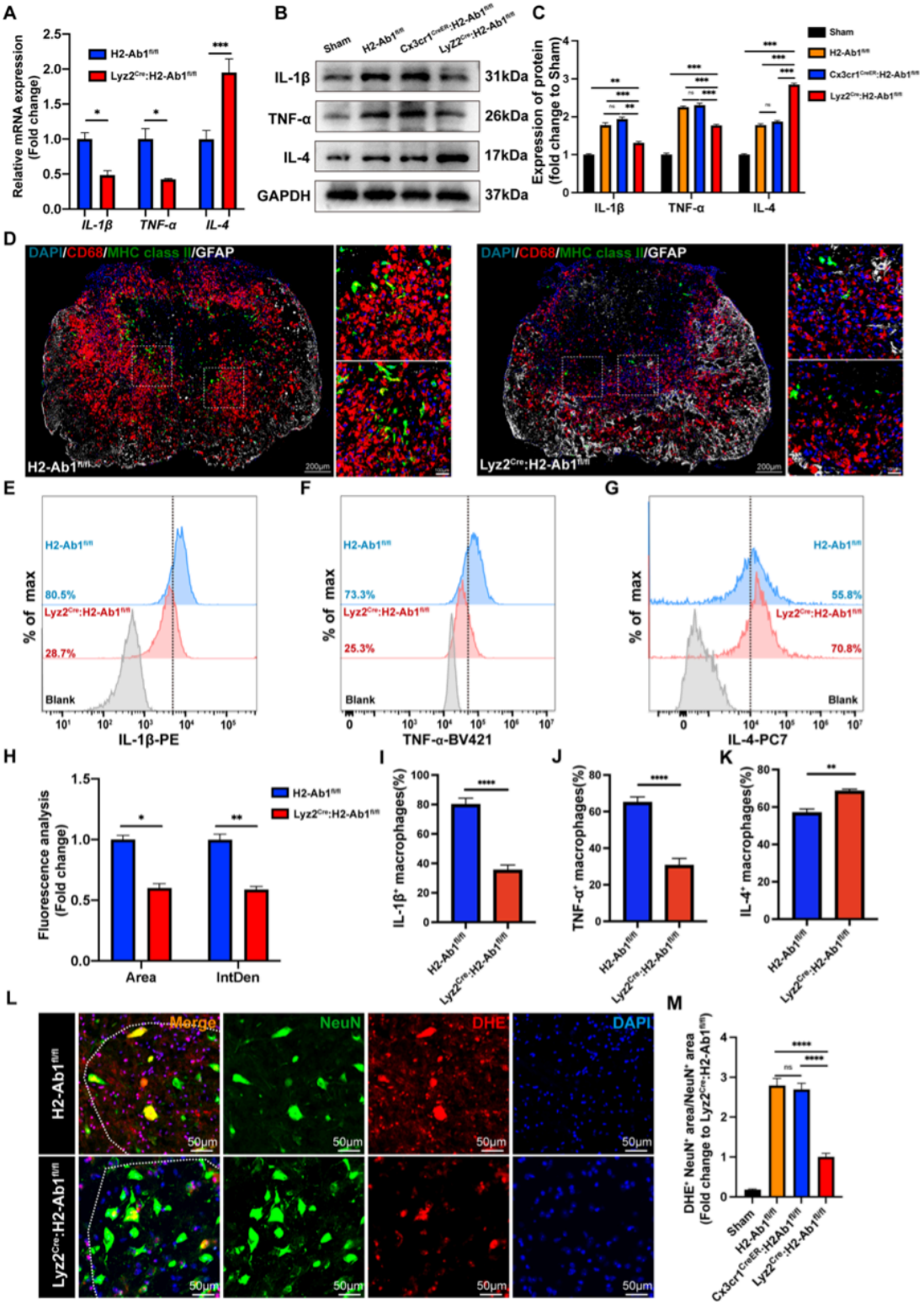


Figure 7

Knockout *H2-Ab1* in macrophages ameliorates local inflammation after SCI.

A qPCR analysis of relative mRNA expression of IL-1β, TNF-α, and IL-4. **B** Western blotting showing IL-1β, TNF-α, and IL-4 levels after SCI, with GAPDH as loading control. **C** The optical density values of IL-1β, TNF-α, and IL-4 were quantified and analyzed for each group. n=5. **D** Representative immunostaining of

CD68 and MHC Class II in SCI lesions from the H2-Ab1$^{fl/fl}$ and Lyz2^{Cre}:H2-Ab1$^{fl/fl}$ groups at day 7 following SCI. **E-G** Representative flow cytometry plots of IL-1β (E), TNF-α (F) and IL-4(G) expression in CD45^{hi}CD11b^{+} infiltrating macrophages from H2-Ab1$^{fl/fl}$ and Lyz2^{Cre}:H2-Ab1$^{fl/fl}$ mice at acute SCI (7 dpi). **H** Quantization of fluorescence area and total fluorescence intensity of CD68 in (D). **I-K** Quantification of IL-1β (E), TNF-α (F) and IL-4(G) expression in CD45^{hi}CD11b^{+} infiltrating macrophages from H2-Ab1$^{fl/fl}$ and Lyz2^{Cre}:H2-Ab1$^{fl/fl}$ mice at acute SCI (7 dpi); n=5. **L** Representative image of DHE staining for the H2-Ab1$^{fl/fl}$ and Lyz2^{Cre}:H2-Ab1$^{fl/fl}$ mice. **M** Statistical analysis of the ratio of DHE^{+} NeuN^{+} area to NeuN^{+} area. Data are mean ± SEM. *P < 0.05, **P < 0.01, ***P < 0.001, ****P < 0.0001.

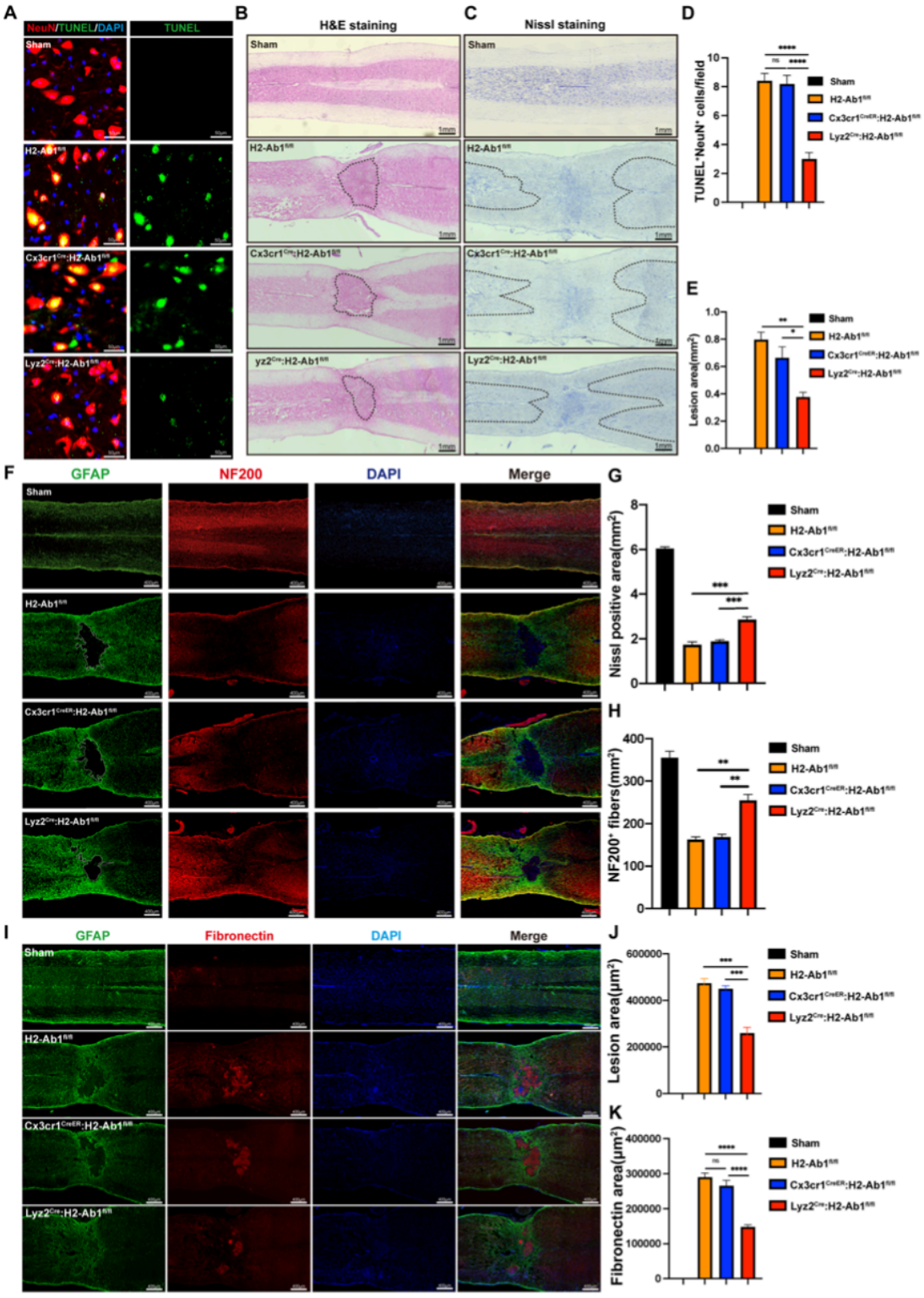


Figure 8

H2-Ab1 knockout in macrophages improves histological findings of SCI.

A The representative images show TUNEL staining in the sham, H2-Ab1$^{fl/fl}$, Cx3cr1^{CreER}:H2-Ab1$^{fl/fl}$, and Lyz2^{Cre}:H2-Ab1$^{fl/fl}$ mice. **B** Representative images show H&E staining after SCI from the sham, H2-Ab1$^{fl/fl}$, Cx3cr1^{CreER}:H2-Ab1$^{fl/fl}$, and Lyz2^{Cre}:H2-Ab1$^{fl/fl}$ mice. **C** Representative images show Nissl staining

after SCI from the sham, H2-Ab1$^{fl/fl}$, Cx3cr1^{CreER}:H2-Ab1$^{fl/fl}$, and Lyz2^{Cre}:H2-Ab1$^{fl/fl}$ mice. **D** The statistical analysis of the results of TUNEL staining is presented in (A). n=5. **E** Quantitative analysis of the lesion area in (B). n=5. **F** Representative immunostaining from sham, H2-Ab1$^{fl/fl}$, Cx3cr1^{CreER}:H2-Ab1$^{fl/fl}$, and Lyz2^{Cre}:H2-Ab1$^{fl/fl}$ mice on day 35 after SCI; Neurofilament indicated by NF200, and astrocytes by GFAP to indicate the lesion area. **G** Quantitative analysis of the Nissl-positive area (mm^2) in (C). n=5 **H** Quantification of NF200 fibers/mm^2 in (F). n=5. **I** Representative immunostaining from sham, H2-Ab1$^{fl/fl}$, Cx3cr1^{CreER}:H2-Ab1$^{fl/fl}$, and Lyz2^{Cre}:H2-Ab1$^{fl/fl}$ mice on day 35 after SCI; fibrous scar indicated by Fibronectin, and astrocytes by GFAP to indicate the lesion area. **J** Quantification of the lesion area in (F). n=5 . **K** Quantification of fibrous scar area in (I). n=5. Data are shown as mean ± SEM. n=5. **P < 0.01, ***P < 0.001, ****P < 0.0001.

Supplementary Files

This is a list of supplementary files associated with this preprint. Click to download.

- Supplementarymaterials.docx
- originalwb.docx
- floatimage9.jpeg